The Effect of Plasma Boundaries on the Dynamic Evolution of Relativistic Radiation Belt Electrons

Dedong Wang[1]*, Yuri Y. Shprits[1,2,3], Irina S. Zhelavskaya[1,2], Frederic Effenberger[1], Angelica Castillo[1,2], Alexander Y. Drozdov[3], Nikita Aseev[1,2], Sebastian Cervantes[1,2]

[1]GFZ German Research Centre for Geosciences, Potsdam, Germany
[2]Institute of Physics and Astronomy, University of Potsdam, Potsdam, Germany
[3]Department of Earth, Planetary, and Space Sciences, University of California, Los Angeles, California, USA

Key Points:

- The plasmapause position plays an important role in radiation belt dynamics.
- The magnetopause shadowing and outward radial diffusion significantly contribute to the net loss of electrons.
- The VERB-3D code reproduces the general dynamics of relativistic electrons during GEM challenge events.

* Corresponding author: Dedong Wang, dedong@gfz-potsdam.de

Abstract

Understanding the dynamic evolution of relativistic electrons in the Earth's radiation belts during both storm and non-storm times is a challenging task. The U.S. National Science Foundation's Geospace Environment Modeling (GEM) focus group "Quantitative Assessment of Radiation Belt Modeling" (QARBM) has selected two storm time and two non-storm time events that occurred during the second year of the Van Allen Probes mission for in-depth study. Here, we perform simulations for these GEM challenge events using the 3-Dimensional Versatile Electron Radiation Belt (VERB-3D) code. We set up the outer L^* boundary using data from Geostationary Operational Environmental Satellites (GOES) and validate the simulation results against satellite observations from both the GOES and Van Allen Probe missions for 0.9 MeV electrons. Our results show that the position of the plasmapause plays a significant role in the dynamic evolution of relativistic electrons. The magnetopause shadowing effect is included by using last closed drift shell (LCDS), and it is shown to significantly contribute to the dropouts of relativistic electrons at high L^*.

1 Introduction

Understanding the dynamic evolution of relativistic electrons in the Earth's radiation belts under different geomagnetic conditions is challenging, due to the delicate balance between various acceleration and loss processes. Different adiabatic and non-adiabatic processes have been proposed to cause the acceleration and loss of relativistic electrons (e.g. Millan & Baker, 2012; Y. Y. Shprits, Elkington, Meredith, & Subbotin, 2008; Y. Y. Shprits, Subbotin, Meredith, & Elkington, 2008; R. M. Thorne, 2010). Adiabatic variations occur when the forces acting on particles remain virtually unchanged on time and spacial scale associated with the adiabatic invariant (e.g. Roederer, 1970; Schulz & Lanzerotti, 1974). During geomagnetic storms, the slow enhancement of the ring current causes the expansion of magnetic field lines in the inner magnetosphere inside the peak of ring current. To conserve the third invariant, electrons move outward. Meanwhile, the first and second invariant are also conserved. This process causes electrons to lose energy and is referred to as the Dst-effect (H.-J. Kim & Chan, 1997). During this process, fixed energy channels of instruments on board satellites observe a decrease of fluxes. Adiabatic changes are reversible, and the flux of electrons with a certain energy can be recovered after the storm. In addition to adiabatic variations, there are also non-adiabatic changes.

Several nonadiabatic processes are proposed to account for loss and acceleration of the radiation belt electrons. There are various plasma waves with frequencies comparable to the frequencies associated with the adiabatic motions (e.g. Roederer, 1970; Schulz & Lanzerotti, 1974). These waves can violate the adiabatic invariant and cause non-adiabatic changes of particles. For example, ultra-low frequency (ULF) waves oscillate with a similar frequency to the timescale of the drift motion of particles. Therefore, ULF waves can violate the third adiabatic invariant of particles, thus driving inward or outward radial diffusion of particles and causing acceleration or deceleration of particles (e.g. Fälthammar, 1965; Fu, Cao, Yang, & Lu, 2011; Lyons & Thorne, 1973; Ozeke, Mann, Murphy, Jonathan Rae, & Milling, 2014; Y. Shprits & Thorne, 2004). Coupled with the magnetopause shadowing effect, which generates a sharp gradient near the boundary, ULF waves can drive particle motion outward and finally result in loss to the magnetopause (Y. Shprits et al., 2006). Electromagnetic ion cyclotron (EMIC) waves are suggested to cause fast loss of radiation belt electrons (R. M. Thorne & Kennel, 1971). The minimum resonance energies of electrons are higher than 2 MeV in most cases (e.g. Cao, Shprits, Ni, & Zhelavskaya, 2017; L. Chen, Zhu, & Zhang, 2019; Drozdov, Shprits, Usanova, et al., 2017; Ni et al., 2018; Y. Y. Shprits et al., 2016, 2013). Very Low Frequency (VLF) waves oscillate at frequencies similar to the frequencies of the gyration and bounce motion of particles. Thus, VLF waves can cause local diffusion in pitch angle and energy, which may lead to the precipitation or enhancement of radiation belt electrons (e.g. R. Horne & Thorne, 2003; R. B. Horne & Thorne, 1998). For example, outside the plasmasphere, chorus waves are believed to play an important dual role in both the enhancement and precipitation of electrons (e.g. R. M. Thorne, 2010). Inside the plasmasphere, plasmaspheric hiss waves can cause the slow decay of radiation belts electrons with loss time scales on the order of 5 to 10 days (e.g. Lyons, Thorne, & Kennel, 1972; Orlova, Spasojevic, & Shprits, 2014). In general, the plasmapause separates chorus waves outside the plasmasphere and hiss waves inside the plasmasphere.

"To concentrate community efforts and maximize scientific returns", the U.S. National Science Foundation's Geospace Environment Modeling (GEM) focus group "Quantitative Assessment of Radiation Belt Modeling" (QARBM) has selected two storm time and two non-storm time events that occurred during the second year of the Van Allen Probes mission for in-depth study (Tu, Li, Albert, & Morley, 2019). A number of studies have been performed for these GEM challenge events (Tu et al., 2019, and references

therein). In particular, the storm time enhancement event on March 17, 2013 has been extensively studied using methods of both observations (e.g. Baker et al., 2014; Boyd et al., 2014; Foster et al., 2014, 2017; Olifer, Mann, Morley, Ozeke, & Choi, 2018) and simulations, including Fokker-Planck, Magnetohydrodynamics (MHD), and test particle simulations, based on both quasi-linear and non-linear theories (e.g. Aseev et al., 2019; Hudson et al., 2015; Kubota & Omura, 2018; Li et al., 2014; Ma et al., 2018; Y. Y. Shprits et al., 2015; Xiao et al., 2014). These studies suggest that chorus waves play a crucial role in the enhancement of radiation belt electrons during this event. For example, by exploring the phase space density (PSD) profile of electrons at different energies, Boyd et al. (2014) suggest that, during this event, electrons with first adiabatic invariant (μ) lower than 200 MeV/G have a source in the plasmasheet. After their injection and radial diffusion into the inner magnetosphere, it is very likely that they are accelerated by chorus waves to higher μ. Xiao et al. (2014) performed 2-D simulations to check the effect of intensified chorus waves observed by Van Allen Probes, and they found that those chorus waves account for the enhancement of relativistic electrons at $L = 4.5$. By performing 2-D simulations using a chorus wave distribution inferred from low altitude satellite measurements, Li et al. (2014) showed that chorus-driven acceleration can explain the observed peak in the electron PSD at $L = 4.25$. By performing Versatile Electron Radiation Belt-4D (VERB-4D) simulations, which combine convective and diffusive processes, Y. Y. Shprits et al. (2015) reproduced the enhancement of electrons at energies of 0.2 MeV, 0.4 MeV, 0.7 MeV and 1 MeV on March 17, 2013. The storm time dropout event on 1 June 2013 has been studied by Kang et al. (2018) using the Comprehensive Inner Magnetosphere-Ionosphere (CIMI) model. They suggested that the magnetopause shadowing effect and the outer radial diffusion resulted in the flux dropout of energetic electrons. The effects of chorus waves and hiss waves are not included in their work. For the nonstorm time dropout event on September 24, 2013, Su et al. (2016) performed 3-D simulations and suggested that this dropout is mainly caused by wave-induced precipitation by plasmaspheric hiss waves and EMIC waves. For the nonstorm time enhancement event on September 19, 2013, Ma et al. (2018) conducted 3-D simulations for two days (September 19, 2013 and September 20, 2013). Their results show that the incorporation of both radial diffusion and local diffusion reasonably reproduces the observed location and magnitude of electron flux enhancements. In their study, they used Van Allen Probes observations to set up initial conditions, lower ($L = 2.5$) and upper ($L = 6$)

L-shell boundaries, which are very close to the region where enhancement happens ($5 \leq L \leq 6$). They also used Van Allen Probe measurements to update the lower and upper energy boundaries, which are from 104 keV to 5.23 MeV at $L = 6$ and from 300 keV to 10 MeV at $L = 4$. These boundaries are close to the energy and L range where enhancements of electron flux are observed during the nonstorm event, and as a result, the data-driven boundaries may be a contributing factor. In addition, event-specific wave distributions inferred from low altitude satellites measurements are also adopted in their study.

In the present study, we extend previous works on these GEM challenge events by performing simulations using the VERB-3D code to investigate the effects of the plasmapause and magnetopause locations on the dynamic evolution of relativistic electrons in the outer radiation belt. Our current study differs from aforementioned simulation papers about these GEM Challenge Events in the following aspects:

- None of these previous studies investigated the four events in a single paper. Here, we systematically perform 3-D simulations for these events.
- None of the previous studies performed simulations to investigate the effect of magnetopause shadowing effect using last closed drift shell for these events.
- None of the previous studies investigated the effect of plasmapause position on the dynamic evolution of relativistic electrons.
- Most of these previous modeling studies of the GEM Challenge Events set up boundaries using Van Allen Probe data that are very close to the energies and L-shells of interest. Such introduction of Van Allen Probe data at lower and upper energy boundaries, initial conditions, lower and higher L-shell boundaries, may affect the simulation results and may make it difficult to distinguish the results of the physics based modeling from simple propagation of satellite data from the boundaries. In our current study, instead of using Van Allen Probe measurements to set up the upper L boundary at $L = 5.5$, we use measurements from GOES satellites at GEO, which is the only data-driven boundary in our simulations. In this way we analyze the results of the simulations in the regions sufficiently far away from any data-driven boundary. Extending the outer boundary to a region further from the Earth can lead to a better understanding of the effect of the competing processes, especially between radial and local diffusion. It can be also helpful to determine which

mechanism is dominant and to objectively judge the performance of the modeling codes.

- Most of these previous simulation studies for the GEM Challenge Events used event-specified wave data, either taken from Van Allen Probe in-situ observation or inferred from low Earth orbit satellites. In-situ wave measurements from Van Allen Probes cannot provide the global distribution of waves in each event. Wave distribution inferred from low Earth orbit (LEO) satellites such as POES can provide global parameters of waves (Y. Chen, Reeves, Friedel, & Cunningham, 2014; Li et al., 2013; Ni et al., 2014). This technique has been validated in several event studies (e.g. Ma et al., 2018; R. Thorne et al., 2013; Tu et al., 2014) and needs further tests using accumulated data sets of conjugate observations of waves and precipitations. In particular, due to the finite field of view (FOV) of the instrument, it is not easy to distinguish precipitated particles from trapped particles. Even a small portion of the trapped population inside the FOV of the instrument can significantly affect the analysis of the precipitation. Moreover, geographic changes in the magnetic field at LEO may introduce additional uncertainties. As models often consider only the ratio of 0° to 90° detector measurements, such ratio may appear not to be always representative of the wave activity. In this study, instead of using event specific waves, we use empirical wave models.

Our paper is organized as follows: first, we describe the VERB-3D code and the parameters adopted for our numerical simulations in section 2. Then in section 3, we present simulation results and their validation against satellite observations. Results and other possible mechanisms are discussed in section 4. Finally, we summarize our findings and outline directions for future studies in section 5.

2 Model Description

The dynamic evolution of electrons in the radiation belts can be described by the bounce- and Magnetic Local Time (MLT)-averaged Fokker-Planck equation (e.g., Schulz & Lanzerotti, 1974; Y. Y. Shprits, Subbotin, & Ni, 2009):

$$\frac{\partial f}{\partial t} = L^{*2}\frac{\partial}{\partial L^*}\bigg|_{\mu,J}\left(\frac{1}{L^{*2}}D_{L^*L^*}\frac{\partial f}{\partial L^*}\bigg|_{\mu,J}\right) + \frac{1}{p^2}\frac{\partial}{\partial p}\bigg|_{\alpha_0,L^*} p^2\left(D_{pp}\frac{\partial f}{\partial p}\bigg|_{\alpha_0,L^*} + D_{p\alpha_0}\frac{\partial f}{\partial \alpha_0}\bigg|_{p,L^*}\right) + \frac{1}{T(\alpha_0)\sin(2\alpha_0)}\frac{\partial}{\partial \alpha_0}\bigg|_{p,L^*} T(\alpha_0)\sin(2\alpha_0)\left(D_{\alpha_0\alpha_0}\frac{\partial f}{\partial \alpha_0}\bigg|_{p,L^*} + D_{\alpha_0 p}\frac{\partial f}{\partial p}\bigg|_{\alpha_0,L^*}\right) - \frac{f}{\tau_{lc}}, \tag{1}$$

where f is the electron PSD; t is time; μ and J are the first and second adiabatic invariant; L^* is inversely proportional to the third adiabatic invariant; p is the relativistic momentum of electrons; α_0 is the equatorial pitch angle of particles; $T(\alpha_0)$ is a function related to the bounce frequency and can be approximated as (Lenchek & Singer, 1962)

$$T(\alpha_0) = 1.3802 - 0.3198(\sin\alpha_0 + \sin^{1/2}\alpha_0); \tag{2}$$

and $D_{L^*L^*}$, D_{pp}, $D_{p\alpha_0}$, $D_{\alpha_0 p}$, and $D_{\alpha_0\alpha_0}$ in equation (1) are the bounce- and MLT- averaged scattering rates (or diffusion coefficients) due to resonant wave-particle interactions. τ_{lc} in equation (1) is the lifetime parameter accounting for losses of particles inside the loss cone due to collisions with atmospheric neutrals. In this study, the lifetime τ_{lc} is set to a quarter of a bounce period for electrons inside the loss cone and infinity outside the loss cone.

2.1 Diffusion Coefficients

The radial diffusion coefficient due to interactions with ULF waves is adopted from Brautigam and Albert (2000):

$$D_{L^*L^*}(\mathrm{Kp}, L^*) = 10^{(0.506\mathrm{Kp}-9.325)} L^{*10}. \tag{3}$$

This parameterization is valid for $\mathrm{Kp} \leq 6$. In this study, however, we extrapolate it also to larger Kp values. Similar results are obtained using the radial diffusion coefficients from Ozeke et al. (2014) (not shown). For readers' interest, similar VERB-3D simulation results were show in Drozdov, Shprits, Aseev, Kellerman, and Reeves (2017) using radial diffusion coefficients from Brautigam and Albert (2000) and Ozeke et al. (2014). Bounce- and MLT-averaged diffusion coefficients D_{pp}, $D_{p\alpha_0}$, $D_{\alpha_0 p}$, and $D_{\alpha_0\alpha_0}$ are calculated using the Full Diffusion Code (FDC) (Y. Y. Shprits & Ni, 2009; Y. Y. Shprits et al., 2009). The FDC is capable of calculating resonant scattering rates including first-order, Landau, and higher order resonance by obliquely propagating waves. For the bounce-average process, Orlova and Shprits (2011) developed a method for removing the integrand's singularity through a change of variables. Calculation of the diffusion coefficients requires wave models depending on spatial variables, such as MLT, latitude, L, and geomagnetic conditions. For the amplitude and frequency distribution of chorus waves, we use a newly developed model based on five years of Van Allen Probe data (Wang et al., 2019). For the wave normal angle (θ) distribution of chorus waves, we use a frequently adopted model, that is, $\theta_{lc} = 0°,\ \theta_{uc} = 45°,\ \theta_m = 0°$, and $\theta_w = 30°$, where θ_m is the

peak value of wave normal angle, θ_w is the width of the angle, and θ_{lc} and θ_{uc} are the lower and upper cut-off to the wave normal angle distribution, outside which the wave power is zero (e.g. K.-C. Kim, Shprits, Subbotin, & Ni, 2012; R. Thorne et al., 2013). For plasmaspheric hiss waves, we are also using a model developed based on Van Allen Probe observations (Orlova, Shprits, & Spasojevic, 2016; Spasojevic, Shprits, & Orlova, 2015). In this study, we assume local diffusion due to chorus waves outside the plasmasphere and due to hiss waves inside the plasmasphere. Plasma densities inside the plasmasphere are calculated according to Denton et al. (2006) and plasma densities outside the plasmasphere are estimated from Sheeley, Moldwin, Rassoul, and Anderson (2001). We also include lightning whistlers with the same parameterization as in K.-C. Kim et al. (2012). EMIC waves mainly affect electrons with energy higher than a few MeV. Therefore, effects of EMIC waves are not included in our simulations since we focus on the dynamics of electrons with energy of 0.9 MeV in this study. For readers' interest, observations and simulations for 0.5 MeV electrons during these events are shown in the supporting material.

2.2 Boundary and Initial Conditions

In our simulations, six boundary conditions and one initial condition are set up as follows:

- Lower L^* boundary: the PSD of electrons at the lower L^* boundary for the radial diffusion operator is set to be zero at $L^* = 1.0$ to represent losses to the atmosphere.
- Upper L^* boundary: the PSD variation at the outer boundary ($L^* = 6.6$) is calculated using GOES measurements, following the approach described in Wang and Shprits (2019).
- Boundary conditions for the pitch-angle operator are $f(\alpha = 0.7^\circ) = 0$ and $\partial f/\partial\alpha(\alpha = 89.3^\circ) = 0$.
- For the energy diffusion operator, the electron PSD at the lower boundary is set to be constant at 10 keV at $L^* = 6.6$ and extend to lower L^* to simulate a balance between convective sources and losses.
- The PSD at the upper energy boundary is set to be zero at 10 MeV at $L^* = 6.6$ assuming an absence of such high energy electrons at $L^* = 6.6$.

- The initial condition is set up using a steady state solution (Y. Shprits & Thorne, 2004).

2.3 Modeling Methodology

Technical details of the VERB-3D code can be found in previous studies (e.g. Castillo et al., 2019; Drozdov, Shprits, Aseev, et al., 2017; K.-C. Kim et al., 2012; Y. Y. Shprits et al., 2009; Subbotin, Shprits, & Ni, 2011). The numerical grid used in our simulations in this study is 29×101×91, uniform in L^*, and logarithmic in energy and pitch-angle. Several factors are taken into account in our simulations:

(1) The plasmapause location separates chorus waves outside of the plasmasphere and hiss waves inside the plasmasphere. We use two different methods to obtain the plasmapause position for each timestep of the simulations. One method is to calculate the plasmapause position using the time series of the Kp index according to Carpenter and Anderson (1992):

$$L_{pp} = 5.6 - 0.46\mathrm{Kp}_{\max}, \tag{4}$$

where L_{pp} is the L-shell value of the plasmapause and Kp_{max} is the maximum Kp value over the previous 24 hours. This empirical plasmapause model is limited to a minimum $L_{pp} = 2$ at $\mathrm{Kp}_{\max} \geq 7$. During the event periods under study here, the maximum $\mathrm{Kp}_{\max}$ value is 7. The other method to obtain the plasmapause position is using a recently developed Plasma density in the Inner magnetosphere Neural network-based Empirical (PINE) model (Zhelavskaya, Shprits, & Spasojevic, 2017, 2018; Zhelavskaya, Spasojevic, Shprits, & Kurth, 2016). The PINE density model was developed using neural networks and was trained on the electron density data set from the Van Allen Probes Electric and Magnetic Field Instrument Suite and Integrated Science (EMFISIS) (Kletzing et al., 2013). The model reconstructs the plasmasphere dynamics well (with a cross-correlation of 0.95 on the test set), and its global reconstructions of plasma density are in good agreement with the IMAGE EUV images of global distribution of He^+. We calculated the MLT-averaged plasmapause position using the output of the PINE model by applying a density threshold of 40 cm^{-3} to separate the plasmasphere from the outside of the plasmasphere.

(2) The last closed drift shell (L^*_{LCDS}) is calculated using the IRBEM library (Boscher, Bourdarie, O'Brien, & Guild, 2010) and TS07D magnetic field model (Tsyganenko & Sit-

nov, 2007) and then used to simulate the effect of magnetopause shadowing. When L^* is larger than the last closed drift shell location, we set the PSD to zero before the step of radial diffusion in the simulation.

2.4 Validation Methodology

We validate our simulation results against satellite observations, which allows us to examine the extent to which the observed flux can be explained by the proposed mechanism and to test the effect of plasma boundaries. Particle measurements from both Van Allen Probes and GOES are used. The Magnetic Electron Ion Spectrometer (MagEIS) instruments on board the Van Allen Probes measure electrons with energies from 20 keV to 4.8 MeV (Blake et al., 2013). To quantify the difference between the simulation results and the observations, we use the difference normalized by the maximum average of observed flux (J_O) and simulated flux (J_S) for each eight hours ($\mathrm{ND}_{\max}(L^*,t)$), which is defined as:

$$\mathrm{ND}_{\max}(L^*,t) = \frac{J_S(L^*,t) - J_O(L^*,t)}{\max|_{\text{over } L^* \text{ every 8 hours}} \frac{J_S(L^*,t)+J_O(L^*,t)}{2}}. \tag{5}$$

We choose eight hours as a period for calculating maximum average due to the fact that Van Allen Probes fly through all L-shells in approximately eight hours.

3 Comparison of Simulations With Observations

Figures 1-3 compare the simulated fluxes to the observed fluxes from both Van Allen Probes and GOES, for the considered GEM challenge events. In each figure, panel (a) shows the observed flux of electrons with energy at 0.9 MeV and an equatorial pitch-angle of 50°, as a function of L^* and time. Here, L^* is calculated using the TS07D magnetic field model (Tsyganenko & Sitnov, 2007). Data from GOES and Van Allen Probes are consistent with each other at conjunction points. Panels (b) and (c) show the VERB-3D simulation results using plasmapause positions estimated following Carpenter and Anderson (1992) and calculated from the PINE plasmasphere model (Zhelavskaya et al., 2017), respectively. Panels (d) and (e) show the normalized differences between observations and simulation results using different plasmapause positions. Blue color means that the simulation results underestimate the flux, while red and yellow colors indicate that the simulation results overestimate the fluxes. The locations of the plasmapause are overplotted as black lines in panels (b) and (c) and as green lines in panels (d) and (e). The positions of the last closed drift shell calculated using the TS07D magnetic field model

are overplotted as magenta lines in panels (b)-(e). Panel (f) in each figure plots the variation of the Dst (red) and Kp (blue) geomagnetic indices.

3.1 Events 1 and 2: Nonstorm Time Enhancement and Dropout

Figure 1 shows the electron flux observations and VERB-3D simulation results for the period from September 7, 2013 to September 26, 2013, which includes two nonstorm GEM Challenge events: a nonstorm time enhancement event on September 20, 2013 and a nonstorm time dropout event on September 24, 2013. Figure 1(a) illustrates that both GOES and Van Allen Probes observed a significant enhancement of relativistic electrons on September 19-20, 2013, which is followed by a dropout at higher L-shells ($L^* > 5$) and a moderate decrease near L^* of 5 on September 24, 2013. Figure 1(b) shows simulation results using the plasmapause positions estimated following Carpenter and Anderson (1992). It can be seen from Figure 1(d) that during the first day under study, some underestimations occur in the heart of the belt (near $L^* = 5$), which shows that the assumed initial condition does not match very well with the observations. However, during the following day, the simulation results already agree well with the data. During the following eight days, from September 11 to September 19, simulation results reproduced the dropouts at higher L-shells when $L^* > L^*_{\mathrm{LCDS}}$. However, in the heart of the belt, overestimation occurs. This can be associated with the plasmapause location. Outside the plasmapause, chorus wave acceleration leads to overestimation. The other possible reason is that the loss caused by hiss waves inside the plasmapause was not strong enough in the simulation. Thus, the enhancement in the heart of the belt on September 20, 2013 is not very pronounced in this simulation, as shown in Figure 1(b). It can be seen from Figure 1(c) and (e) that using the new plasmapause location improved the agreement between observations and simulations significantly. There is still some overestimation, which may result from the diffusion coefficients of hiss waves. For the dropout event during September 24, the dropout at higher L-shells is reproduced in both simulations by involving the magnetopause shadowing effect. However, a decrease of flux at L-shell range from 4 to 5 is not well reproduced, which will be discussed in section 4.

3.2 Event 3: Storm Time Dropout

On June 1, 2013, a strong geomagnetic storm happened with a minimum Dst index of -110 nT and a maximum Kp index of 7. An electron flux dropout occurred on June

1, 2013, as shown in Figure 2(a). During this period, GOES 13 data is not available. Panels (b) and (c) show results of VERB-3D simulations using different plasmapause positions (overplotted as black lines). The overplotted magenta lines give the LCDS locations calculated in TS07D magnetic field model. It can be seen, using the positions of the LCDS, that the simulation can reproduce the dropouts outside the LCDS well. However, the simulation results did not reproduce the dropout where $L^* < L^*_{LCDS}$ during the storm main phase and exhibit overestimation during the recovery phase. This overestimation may be attributed to errors in the magnetic field model, miss of other loss mechanisms such as wave-particle interaction in plasmaspheric plumes, or underestimated outward radial diffusion rates during these periods. The simulation results using the plasmapause position following Carpenter and Anderson (1992) have some overestimations before the storm near $L^* = 4$. When using the plasmapause estimated from the new PINE plasmasphere model, the agreement between simulation results and observations is improved.

3.3 Event 4: Storm Time Enhancement

On March 17, 2013, a strong storm occurred with a minimum Dst index of -130 nT and a maximum Kp index of 7- as shown in Figure 3(f). During this day, after a sharp dropout across a wide L^* range, the flux of relativistic electrons recovered and enhanced significantly by 2 orders of magnitude at L^* from 3 to 5. Figure 3(a) shows GOES and Van Allen Probes measurements of electrons with energies at 0.9 MeV and pitch-angles at 50°. Before 12:00 UT on March 17, the fluxes of relativistic electrons were dramatically depleted, especially at high L-shells ($L^* \geq 5$). This depletion is suggested to result from the magnetopause shadowing effect (Baker et al., 2014; Li et al., 2014; Olifer et al., 2018). However, previous simulation studies for this event did not investigate the effect of magnetopause shadowing.

In our simulations, we include the effect of magnetopause shadowing to investigate the reason for the sharp dropout before the enhancement event and test the influence of the different plasmapause positions. In addition, instead of using event-specific chorus waves from observations, in our simulations, we use a statistical chorus wave model which was developed using five years of Van Allen Probe data (Wang et al., 2019). Figures 3(b) and 3(c) show the results of VERB-3D simulations using different plasmapause positions. As seen readily in these figures, the depletion of electron fluxes can be well

reproduced by the loss to the last closed drift shell (indicated as overplotted magenta lines). After this depletion, the flux of relativistic electrons enhanced by nearly 2 orders of magnitude during the 12 hours interval on March 17 in the L-shell range [3, 5]. The peak location of the outer radiation belt moves Earthward compared with the location before this storm. The simulation results indicate that the enhancement of relativistic electrons is well reproduced.

4 Discussion

The enhancement and the dropout events during the end of September in 2013 are selected by the GEM Focus Group QARBM as nonstorm time challenge events based on the Dst index. However, the Kp index increased to 4 at both enhancement and dropout time. This indicates that much of the dynamics of the relativistic radiation belts is better organized by the Kp index, rather than by the Dst index, as discussed in Borovsky and Shprits (2017).

During several hours on September 24, 2013, the radiation belt electrons with energy from 500 keV to several MeV exhibited a significant dropout at higher L-shells ($L^* > 5$) and a moderate decrease near L^* of 5. Our simulations incorporate the magnetopause shadowing effect by using the last closed drift shell reproduced the dropout at higher L-shells. However, a decrease of flux at L-shell range from 4 to 5 is not well reproduced. This may result from underestimation of outward radial diffusion, or lack of wave-particle interactions in plasmaspheric plumes. On the other hand, EMIC waves are observed during the interval of this dropout. Su et al. (2016) suggested that this dropout is mainly caused by wave-induced precipitation by plasmaspheric hiss waves and EMIC waves. Using a cold plasma approximation and setting the upper cut-off frequency of EMIC waves at $0.98 f_{\mathrm{cHe^+}}$, the minimum resonant energy of electrons were calculated to extend to as low as 400 keV in their study. However, taking hot plasma effects into account, the minimum resonance energies of electrons interacting with EMIC waves are found to be generally higher than 1 MeV (Cao et al., 2017). By analyzing the wave number of observed EMIC waves and calculating the minimum resonance energy, L. Chen et al. (2019) found that during this event, the minimum resonance energy between EMIC waves and electrons is higher than 16 MeV (see their supporting information). Thus, the effects of EMIC waves in this dropout event are still under debate. Using satellite and ground observations, Engebretson et al. (2018) investigated EMIC waves and their effect on radiation

belt electrons for these GEM challenge events. They also investigated phase space densities and pitch-angle distributions of electrons for this event. The dips in phase space density are suggested to be a signature of EMIC caused precipitations (e.g. Aseev et al., 2017; Y. Y. Shprits, Kellerman, Aseev, Drozdov, & Michaelis, 2017). Dips in the PSD profile were found for electrons with energies higher than 2 MeV, but no dips in PSD were found for electrons with energies near 1 MeV. The investigation of the electron depletion at low L-shell during this event will be a subject of the further research.

During storm times, the plasmasphere becomes more asymmetric due to the enhanced convection. During storm times, the plasmasphere is strongly eroded at all MLTs except for the dusk sector, where a bulge or plume is formed and extends further to the noon sector. Plasmaspheric bulge or plumes may form and extend to higher L-shells during storm time. However, in our 3D simulations using the PINE output, the plasmapause positions are averaged over MLT. This may lead to some overestimations of plasmapause positions during storm times, which can lead to an underestimation of the acceleration by chorus waves. In addition, our simulations in this study did not account for hiss waves in the plasmaspheric plume, which may cause some underestimations of losses.

5 Summary and Conclusions

The results of our study show that:

1. The magnetopause shadowing effect plays an important role for dropout at higher L-shells. The last closed drift shell calculated using the TS07D magnetic field model can be used to simulate the magnetopause shadowing effect.
2. The positions of the plasmapause plays an important role in the dynamic evolution of radiation belt electrons, especially during geomagnetically quiet times.
3. Flux measurements from GOES observations can be used to set up outer boundary conditions for the simulation of radiation belts. During times when the Van Allen Probes data is not available, we can still use measurements from GOES to set up outer boundaries and infer the radiation belt dynamics at lower L-shells.

In future studies, we will test the usage of the innermost position of the plasmapause and include plumes by changing the MLT percentage of chorus waves and hiss waves in different time steps of simulations. Additionally, 4D simulations including the MLT

dependence will be performed to check the effect of the MLT-dependent plasmapause positions and plasmaspheric plumes on the dynamic evolution of the radiation belts in detail.

Acronyms

GEM Geospace Environment Modeling

QARBM Quantitative Assessment of Radiation Belt Modeling

VERB-3D code 3-Dimensional Versatile Electron Radiation Belt code

MLT Magnetic Local Time

PP Plasmapause

PSD Phase Space Density

LCDS Last Closed Drift Shell

FDC Full Diffusion Code

PINE Plasma density in the Inner magnetosphere Neural network-based Empirical model

NURD Neural-network-based Upper-hybrid Resonance Determination (NURD) algorithm

Acknowledgments

We acknowledge the Geospace Environment Modeling Focus Group on the "Quantitative Assessment of Radiation Belt Modeling" for motivating this study. We sincerely acknowledge Adam Kellerman for the preparation of the satellite data used and the calculation of the last closed drift shells. We would like to thank Hayley Allison for the useful discussions. This project has received funding from the European Union's Horizon 2020 research and innovation programme under grant agreement No. 637302, NASA H-SR funding NNX15AI94G, and the Helmholtz-Gemeinshaft (HGF) [10.13039/501100001656]. I. Z. was supported by Geo.X, the Research Network for Geosciences in Berlin and Potsdam, under Grant No. SO-087-GeoX. All Van Allen Probes data were accessed through the MagEIS website (https://rbsp-ect.lanl.gov), and we graciously thank the MagEIS instrument team. The Kp index was provided by GFZ Section 2.3 and downloaded from the World Data Center (http://wdc.kugi.kyoto-u.ac.jp/). NURD plasma density data can be downloaded from ftp://ftp.gfz-potsdam.de/home/rbm/NURD/.

References

Aseev, N., Shprits, Y., Drozdov, A., Kellerman, A., Usanova, M., Wang, D., & Zhelavskaya, I. (2017). Signatures of ultrarelativistic electron loss in the heart of the outer radiation belt measured by Van Allen Probes. *Journal of Geophysical Research: Space Physics*, *122*(10), 10–102.

Aseev, N., Shprits, Y., Wang, D., Wygant, J., Drozdov, A., Kellerman, A., & Reeves, G. (2019). Transport and Loss of Ring Current Electrons Inside Geosynchronous Orbit during the 17 March 2013 Storm. *Journal of Geophysical Research: Space Physics*.

Baker, D., Jaynes, A., Li, X., Henderson, M., Kanekal, S., Reeves, G., ... others (2014). Gradual diffusion and punctuated phase space density enhancements of highly relativistic electrons: Van Allen Probes observations. *Geophysical Research Letters*, *41*(5), 1351–1358.

Blake, J., Carranza, P., Claudepierre, S., Clemmons, J., Crain, W., Dotan, Y., ... others (2013). The magnetic electron ion spectrometer (mageis) instruments aboard the radiation belt storm probes (rbsp) spacecraft. In *The van allen probes mission* (pp. 383–421). Springer.

Borovsky, J. E., & Shprits, Y. Y. (2017). Is the dst index sufficient to define all geospace storms? *Journal of Geophysical Research: Space Physics*, *122*(11).

Boscher, D., Bourdarie, S., O'Brien, P., & Guild, T. (2010). Irbem library v4. 3, 2004–2008. *ONERA-DESP, Toulouse France, Aerospace Corporation, Washington, DC*.

Boyd, A. J., Spence, H. E., Claudepierre, S., Fennell, J. F., Blake, J., Baker, D., ... Turner, D. (2014). Quantifying the radiation belt seed population in the 17 March 2013 electron acceleration event. *Geophysical Research Letters*, *41*(7), 2275–2281.

Brautigam, D., & Albert, J. (2000). Radial diffusion analysis of outer radiation belt electrons during the October 9, 1990, magnetic storm. *Journal of Geophysical Research: Space Physics*, *105*(A1), 291–309.

Cao, X., Shprits, Y. Y., Ni, B., & Zhelavskaya, I. S. (2017). Scattering of ultrarelativistic electrons in the van allen radiation belts accounting for hot plasma effects. *Scientific reports*, *7*(1), 17719.

Carpenter, D., & Anderson, R. (1992). An ISEE/whistler model of equatorial elec-

tron density in the magnetosphere. *Journal of Geophysical Research: Space Physics*, *97*(A2), 1097–1108.

Castillo, A. M., Shprits, Y. Y., Ganushkina, N., Drozdov, A., Aseev, N., Wang, D., & Dubyagin, S. (2019). Simulations of the inner magnetospheric energetic electrons using the IMPTAM-VERB coupled model. *Journal of Atmospheric and Solar-Terrestrial Physics*, *191*, 105050. doi: https://doi.org/10.1016/j.jastp.2019.05.014

Chen, L., Zhu, H., & Zhang, X. (2019). Wavenumber Analysis of EMIC Waves. *Geophysical Research Letters*, *46*(11), 5689-5697. doi: 10.1029/2019GL082686

Chen, Y., Reeves, G. D., Friedel, R. H., & Cunningham, G. S. (2014). Global time-dependent chorus maps from low-Earth-orbit electron precipitation and Van Allen Probes data. *Geophysical Research Letters*, *41*(3), 755–761.

Denton, R., Takahashi, K., Galkin, I., Nsumei, P., Huang, X., Reinisch, B., ... Hughes, W. (2006). Distribution of density along magnetospheric field lines. *Journal of Geophysical Research: Space Physics*, *111*(A4).

Drozdov, A., Shprits, Y., Aseev, N., Kellerman, A., & Reeves, G. D. (2017). Dependence of radiation belt simulations to assumed radial diffusion rates tested for two empirical models of radial transport. *Space Weather*, *15*(1), 150–162. doi: 0.1002/2016SW001426

Drozdov, A., Shprits, Y., Usanova, M., Aseev, N., Kellerman, A., & Zhu, H. (2017). EMIC wave parameterization in the long-term VERB code simulation. *Journal of Geophysical Research: Space Physics*, *122*(8), 8488–8501.

Engebretson, M., Posch, J., Braun, D., Li, W., Ma, Q., Kellerman, A., ... others (2018). EMIC wave events during the four GEM QARBM challenge intervals. *Journal of Geophysical Research: Space Physics*, *123*(8), 6394–6423.

Fälthammar, C.-G. (1965). Effects of time-dependent electric fields on geomagnetically trapped radiation. *Journal of Geophysical Research (1896-1977)*, *70*(11), 2503-2516. doi: 10.1029/JZ070i011p02503

Foster, J., Erickson, P., Baker, D., Claudepierre, S., Kletzing, C., Kurth, W., ... others (2014). Prompt energization of relativistic and highly relativistic electrons during a substorm interval: Van Allen Probes observations. *Geophysical Research Letters*, *41*(1), 20–25.

Foster, J., Erickson, P., Omura, Y., Baker, D., Kletzing, C., & Claudepierre, S.

(2017). Van Allen Probes observations of prompt MeV radiation belt electron acceleration in nonlinear interactions with VLF chorus. *Journal of Geophysical Research: Space Physics*, *122*(1), 324–339.

Fu, H., Cao, J., Yang, B., & Lu, H. (2011). Electron loss and acceleration during storm time: The contribution of wave-particle interaction, radial diffusion, and transport processes. *Journal of Geophysical Research: Space Physics*, *116*(A10).

Horne, R., & Thorne, R. (2003). Relativistic electron acceleration and precipitation during resonant interactions with whistler-mode chorus. *Geophysical research letters*, *30*(10). doi: 10.1029/2003GL016973

Horne, R. B., & Thorne, R. M. (1998). Potential waves for relativistic electron scattering and stochastic acceleration during magnetic storms. *Geophysical Research Letters*, *25*(15), 3011–3014. doi: 10.1029/98GL01002

Hudson, M., Paral, J., Kress, B., Wiltberger, M., Baker, D., Foster, J., ... Wygant, J. R. (2015). Modeling CME-shock-driven storms in 2012–2013: MHD test particle simulations. *Journal of Geophysical Research: Space Physics*, *120*(2), 1168–1181.

Kang, S.-B., Fok, M.-C., Komar, C., Glocer, A., Li, W., & Buzulukova, N. (2018). An energetic electron flux dropout due to magnetopause shadowing on 1 June 2013. *Journal of Geophysical Research: Space Physics*, *123*(2), 1178–1190.

Kim, H.-J., & Chan, A. A. (1997). Fully adiabatic changes in storm time relativistic electron fluxes. *Journal of Geophysical Research: Space Physics*, *102*(A10), 22107–22116.

Kim, K.-C., Shprits, Y., Subbotin, D., & Ni, B. (2012). Relativistic radiation belt electron responses to GEM magnetic storms: Comparison of CRRES observations with 3-D VERB simulations. *Journal of Geophysical Research: Space Physics*, *117*(A8). doi: 10.1029/2011JA017460

Kletzing, C., Kurth, W., Acuna, M., MacDowall, R., Torbert, R., Averkamp, T., ... others (2013). The electric and magnetic field instrument suite and integrated science (EMFISIS) on RBSP. *Space Science Reviews*, *179*(1-4), 127–181. doi: 10.1007/s11214-013-9993-6

Kubota, Y., & Omura, Y. (2018). Nonlinear Dynamics of Radiation Belt Electrons Interacting With Chorus Emissions Localized in Longitude. *Journal of Geo-*

physical Research: Space Physics, *123*(6), 4835–4857.

Lenchek, A. M., & Singer, S. F. (1962). Geomagnetically trapped protons from cosmic-ray albedo neutrons. *Journal of Geophysical Research*, *67*(4), 1263–1287.

Li, W., Ni, B., Thorne, R., Bortnik, J., Green, J., Kletzing, C., ... Hospodarsky, G. (2013). Constructing the global distribution of chorus wave intensity using measurements of electrons by the POES satellites and waves by the Van Allen Probes. *Geophysical Research Letters*, *40*(17), 4526–4532.

Li, W., Thorne, R., Ma, Q., Ni, B., Bortnik, J., Baker, D., ... others (2014). Radiation belt electron acceleration by chorus waves during the 17 March 2013 storm. *Journal of Geophysical Research: Space Physics*, *119*(6), 4681–4693.

Lyons, L. R., & Thorne, R. M. (1973). Equilibrium structure of radiation belt electrons. *Journal of Geophysical Research (1896-1977)*, *78*(13), 2142-2149. doi: 10.1029/JA078i013p02142

Lyons, L. R., Thorne, R. M., & Kennel, C. F. (1972). Pitch-angle diffusion of radiation belt electrons within the plasmasphere. *Journal of Geophysical Research (1896-1977)*, *77*(19), 3455-3474. doi: 10.1029/JA077i019p03455

Ma, Q., Li, W., Bortnik, J., Thorne, R., Chu, X., Ozeke, L., ... others (2018). Quantitative evaluation of radial diffusion and local acceleration processes during GEM challenge events. *Journal of Geophysical Research: Space Physics*, *123*(3), 1938–1952.

Millan, R., & Baker, D. (2012). Acceleration of particles to high energies in Earths radiation belts. *Space Science Reviews*, *173*(1-4), 103–131. doi: 10.1007/s11214-012-9941-x

Ni, B., Cao, X., Shprits, Y. Y., Summers, D., Gu, X., Fu, S., & Lou, Y. (2018). Hot plasma effects on the cyclotron-resonant pitch-angle scattering rates of radiation belt electrons due to EMIC waves. *Geophysical Research Letters*, *45*(1), 21–30.

Ni, B., Li, W., Thorne, R. M., Bortnik, J., Green, J. C., Kletzing, C. A., ... Soria-Santacruz Pich, M. (2014). A novel technique to construct the global distribution of whistler mode chorus wave intensity using low-altitude POES electron data. *Journal of Geophysical Research: Space Physics*, *119*(7), 5685–5699.

Olifer, L., Mann, I. R., Morley, S. K., Ozeke, L. G., & Choi, D. (2018). On the role

of last closed drift shell dynamics in driving fast losses and Van Allen radiation belt extinction. *Journal of Geophysical Research: Space Physics*, *123*(5), 3692–3703.

Orlova, K., & Shprits, Y. (2011). On the bounce-averaging of scattering rates and the calculation of bounce period. *Physics of Plasmas*, *18*(9), 092904.

Orlova, K., Shprits, Y., & Spasojevic, M. (2016). New global loss model of energetic and relativistic electrons based on Van Allen Probes measurements. *Journal of Geophysical Research: Space Physics*, *121*(2), 1308–1314.

Orlova, K., Spasojevic, M., & Shprits, Y. (2014). Activity-dependent global model of electron loss inside the plasmasphere. *Geophysical Research Letters*, *41*(11), 3744–3751. doi: 10.1002/2014GL060100

Ozeke, L. G., Mann, I. R., Murphy, K. R., Jonathan Rae, I., & Milling, D. K. (2014). Analytic expressions for ULF wave radiation belt radial diffusion coefficients. *Journal of Geophysical Research: Space Physics*, *119*(3), 1587–1605.

Roederer, J. G. (1970). *Dynamics of Geomagnetically Trapped Radiation* (1st ed., Vol. 2). New York: Springer-Verlag Berlin Heidelberg.

Schulz, M., & Lanzerotti, L. J. (1974). *Particle diffusion in the radiation belts* (Vol. 7). Springer Science & Business Media.

Sheeley, B., Moldwin, M., Rassoul, H., & Anderson, R. (2001). An empirical plasmasphere and trough density model: CRRES observations. *Journal of Geophysical Research: Space Physics*, *106*(A11), 25631–25641. doi: 10.1029/2000JA000286

Shprits, Y., & Thorne, R. (2004). Time dependent radial diffusion modeling of relativistic electrons with realistic loss rates. *Geophysical research letters*, *31*(8).

Shprits, Y., Thorne, R., Friedel, R., Reeves, G., Fennell, J., Baker, D., & Kanekal, S. (2006). Outward radial diffusion driven by losses at magnetopause. *Journal of Geophysical Research: Space Physics*, *111*(A11).

Shprits, Y. Y., Drozdov, A. Y., Spasojevic, M., Kellerman, A. C., Usanova, M. E., Engebretson, M. J., ... others (2016). Wave-induced loss of ultra-relativistic electrons in the Van Allen radiation belts. *Nature communications*, *7*, 12883.

Shprits, Y. Y., Elkington, S. R., Meredith, N. P., & Subbotin, D. A. (2008). Review of modeling of losses and sources of relativistic electrons in the outer radiation

belt I: Radial transport. *Journal of Atmospheric and Solar-Terrestrial Physics*, *70*(14), 1679–1693.

Shprits, Y. Y., Kellerman, A., Aseev, N., Drozdov, A. Y., & Michaelis, I. (2017). Multi-MeV electron loss in the heart of the radiation belts. *Geophysical Research Letters*, *44*(3), 1204–1209.

Shprits, Y. Y., Kellerman, A. C., Drozdov, A. Y., Spence, H. E., Reeves, G. D., & Baker, D. N. (2015). Combined convective and diffusive simulations: VERB-4D comparison with 17 March 2013 Van Allen Probes observations. *Geophysical Research Letters*, *42*(22), 9600–9608.

Shprits, Y. Y., & Ni, B. (2009). Dependence of the quasi-linear scattering rates on the wave normal distribution of chorus waves. *Journal of Geophysical Research: Space Physics*, *114*(A11).

Shprits, Y. Y., Subbotin, D., Drozdov, A., Usanova, M. E., Kellerman, A., Orlova, K., ... Kim, K.-C. (2013). Unusual stable trapping of the ultrarelativistic electrons in the Van Allen radiation belts. *Nature Physics*, *9*(11), 699.

Shprits, Y. Y., Subbotin, D., & Ni, B. (2009). Evolution of electron fluxes in the outer radiation belt computed with the VERB code. *Journal of Geophysical Research: Space Physics*, *114*(A11). doi: 10.1029/2008JA013784

Shprits, Y. Y., Subbotin, D. A., Meredith, N. P., & Elkington, S. R. (2008). Review of modeling of losses and sources of relativistic electrons in the outer radiation belt II: Local acceleration and loss. *Journal of Atmospheric and Solar-Terrestrial Physics*, *70*(14), 1694–1713. doi: 10.1016/j.jastp.2008.06.014

Spasojevic, M., Shprits, Y., & Orlova, K. (2015). Global empirical models of plasmaspheric hiss using Van Allen Probes. *Journal of Geophysical Research: Space Physics*, *120*(12), 10–370.

Su, Z., Gao, Z., Zhu, H., Li, W., Zheng, H., Wang, Y., ... others (2016). Nonstorm time dropout of radiation belt electron fluxes on 24 September 2013. *Journal of Geophysical Research: Space Physics*, *121*(7), 6400–6416.

Subbotin, D., Shprits, Y., & Ni, B. (2011). Long-term radiation belt simulation with the VERB 3-D code: Comparison with CRRES observations. *Journal of Geophysical Research: Space Physics*, *116*(A12). doi: 10.1029/2011JA017019

Thorne, R., Li, W., Ni, B., Ma, Q., Bortnik, J., Chen, L., ... others (2013). Rapid local acceleration of relativistic radiation-belt electrons by magnetospheric

chorus. *Nature*, *504*(7480), 411.

Thorne, R. M. (2010). Radiation belt dynamics: The importance of wave-particle interactions. *Geophysical Research Letters*, *37*(22). doi: 10.1029/2010GL044990

Thorne, R. M., & Kennel, C. F. (1971). Relativistic electron precipitation during magnetic storm main phase. *Journal of Geophysical Research (1896-1977)*, *76*(19), 4446-4453. doi: 10.1029/JA076i019p04446

Tsyganenko, N., & Sitnov, M. (2007). Magnetospheric configurations from a high-resolution data-based magnetic field model. *Journal of Geophysical Research: Space Physics*, *112*(A6).

Tu, W., Cunningham, G., Chen, Y., Morley, S., Reeves, G., Blake, J., ... Spence, H. (2014). Event-specific chorus wave and electron seed population models in DREAM3D using the Van Allen Probes. *Geophysical Research Letters*, *41*(5), 1359–1366.

Tu, W., Li, W., Albert, J., & Morley, S. (2019). Quantitative Assessment of Radiation Belt Modeling. *Journal of Geophysical Research: Space Physics*.

Wang, D., & Shprits, Y. Y. (2019). On how high-latitude chorus waves tip the balance between acceleration and loss of relativistic electrons. *Geophysical Research Letters*, *46*(14), 7945-7954. doi: 10.1029/2019GL082681

Wang, D., Shprits, Y. Y., Zhelavskaya, I., Agapitov, O., Drozdov, A., & Aseev, N. (2019). Analytical Chorus Wave Model Derived from Van Allen Probe Observations. *Journal of Geophysical Research: Space Physics*.

Xiao, F., Yang, C., He, Z., Su, Z., Zhou, Q., He, Y., ... others (2014). Chorus acceleration of radiation belt relativistic electrons during March 2013 geomagnetic storm. *Journal of Geophysical Research: Space Physics*, *119*(5), 3325–3332.

Zhelavskaya, I. S., Shprits, Y. Y., & Spasojevic, M. (2017). Empirical modeling of the plasmasphere dynamics using neural networks. *Journal of Geophysical Research: Space Physics*, *122*(11).

Zhelavskaya, I. S., Shprits, Y. Y., & Spasojevic, M. (2018). Reconstruction of Plasma Electron Density From Satellite Measurements Via Artificial Neural Networks. In *Machine learning techniques for space weather* (pp. 301–327). Elsevier.

Zhelavskaya, I. S., Spasojevic, M., Shprits, Y. Y., & Kurth, W. (2016). Automated determination of electron density from electric field measurements on the Van

673 Allen Probes spacecraft. *Journal of Geophysical Research: Space Physics*,
674 *121*(5), 4611–4625. doi: 0.1002/2015JA022132

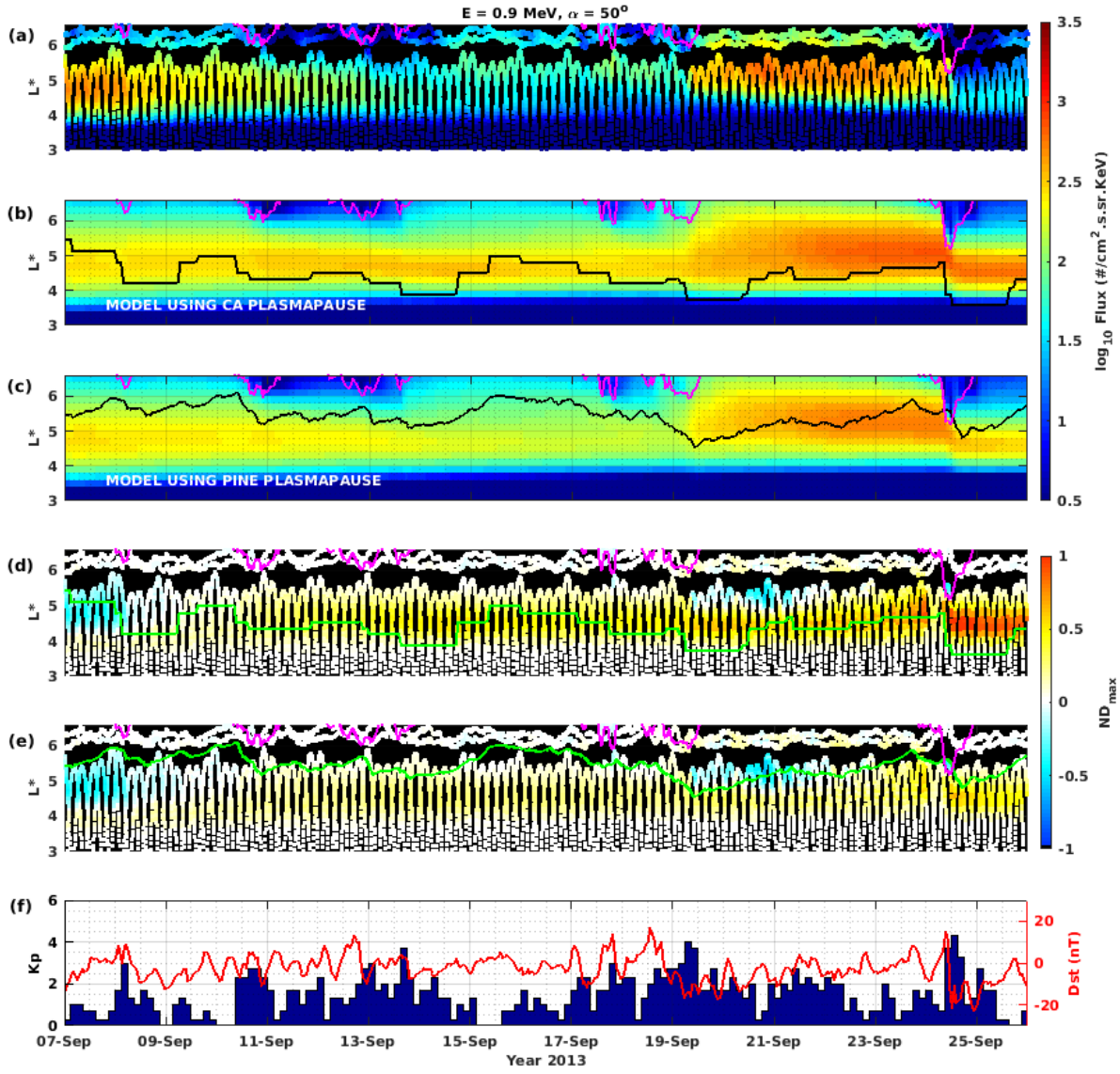

Figure 1. Particle observations and VERB simulations from September 7, 2013 to September 26, 2013 including both nonstorm GEM Challenge events (a nonstorm time enhancement event on September 20, 2013 and a nonstorm time dropout event on September 24, 2013). (a) Particle flux for 0.9 MeV, 50° pitch angle electrons from observations of Van Allen Probes, GOES 13 and 15. (b) VERB-3D simulation results using plasmapause positions calculated following Carpenter and Anderson (1992) for this period. (c) VERB-3D simulation results using the plasmapause position estimated from the new PINE plasmasphere model (Zhelavskaya et al., 2017, 2018). (d) Normalized difference between observations (shown in panel (a)) and simulations (shown in panel (b)). (e) Normalized difference between observations (shown in panel (a)) and simulations (shown in panel (c)). (f) Dst and Kp index during this period. The overplotted magenta lines in panels (b)-(e) show the last closed drift shell. The overplotted black lines in panels (b)-(e) show the plasmapause positions.

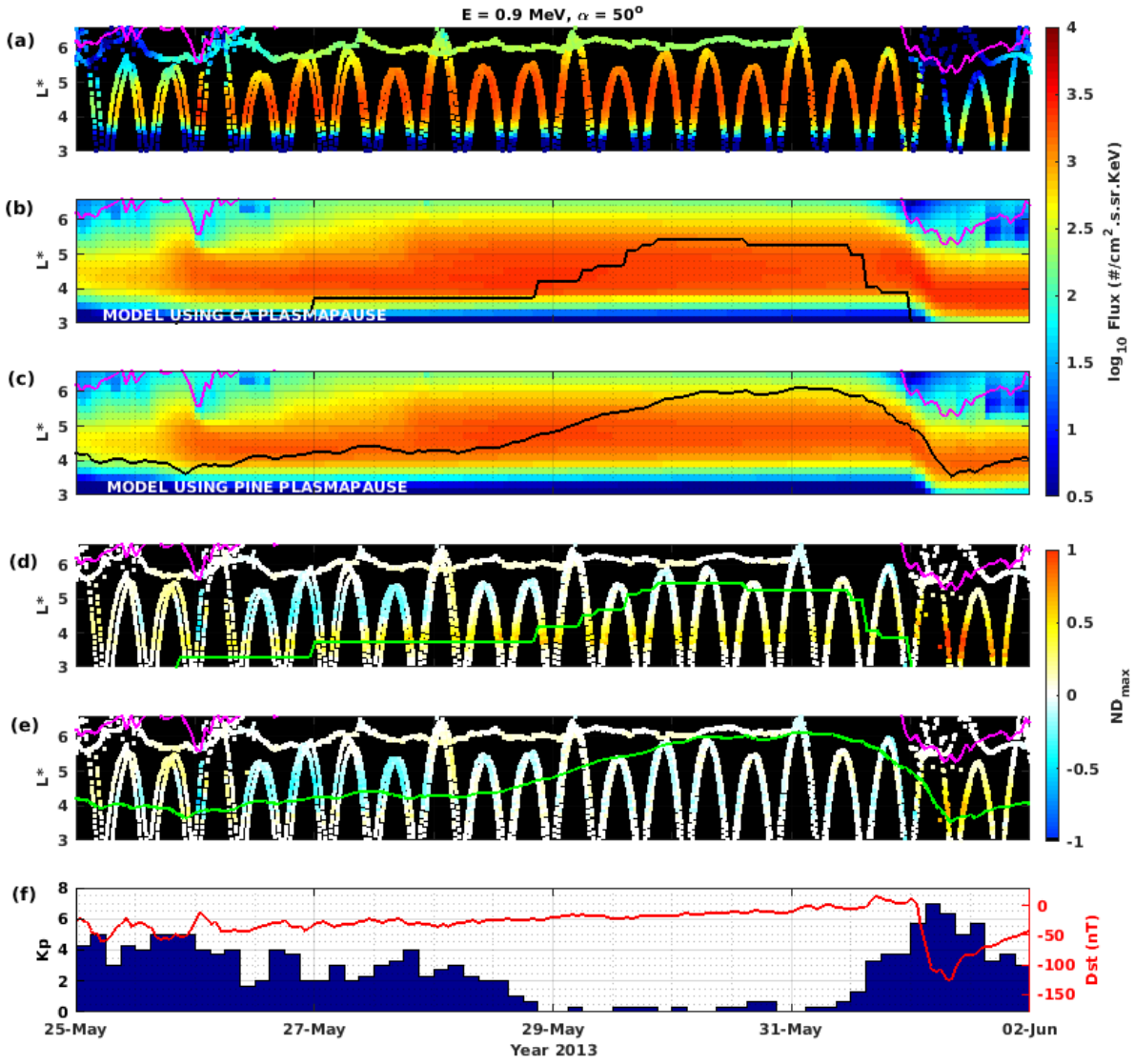

Figure 2. Same format as Figure 1 but for the storm time dropout GEM challenge event (on June 1, 2013) from May 25, 2013 to June 2, 2013.

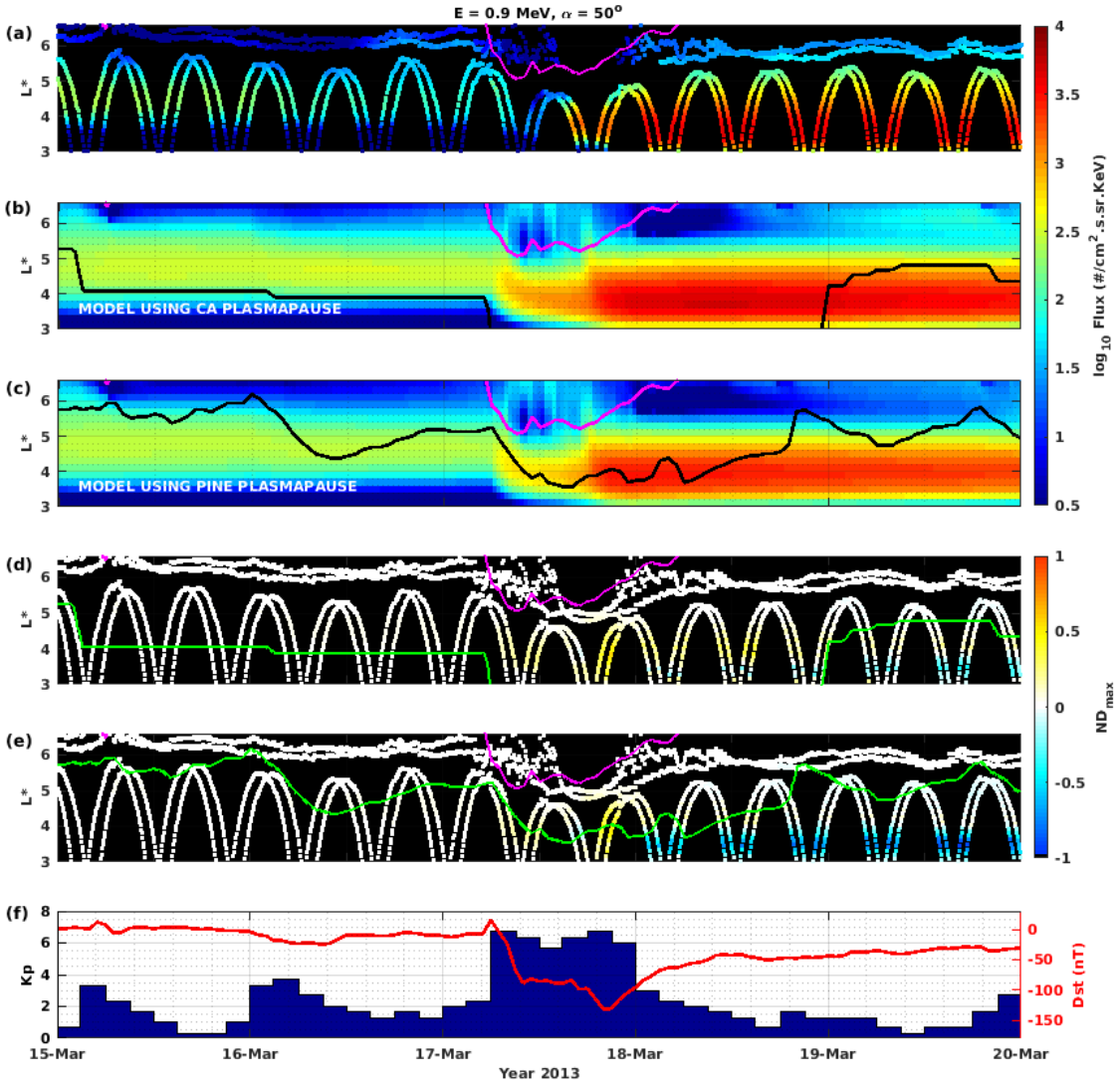

Figure 3. Same format as Figure 1 but for the storm time enhancement GEM challenge event (on March 17, 2013) from Mar 15, 2013 to Mar 20, 2013.